Polarization dependence of soft-x-ray Raman scattering at the L edge of TiO_2

Y. Harada, T. Kinugasa, R. Eguchi, M. Matsubara, and A. Kotani
Institute for Solid State Physics, University of Tokyo, Minato-ku, Tokyo 106-8666, Japan

M. Watanabe and A. Yagishita
Photon Factory, Institute of Materials Structure Science, Tsukuba, Ibaraki 305-0801, Japan

S. Shin
Institute for Solid State Physics, University of Tokyo, Minato-ku, Tokyo 106-8666, Japan
and The Institute of Physical and Chemical Research (RIKEN), Sayo-gun, Hyogo 679-5143, Japan
(Received 18 October 1999)

Polarization dependence of soft-x-ray Raman scattering was investigated at the Ti $2p$ absorption edge of TiO_2. Strong Raman scattering feature appears about 14 eV below elastic peaks with strong polarization dependence. These Raman scattering structures are charge transfer excitations to the antibonding state between $3d^1L^{-1}$ and $3d^0$ states, because they are enhanced when the incident photon energies are tuned at satellite structures of Ti $2p$ absorption spectrum. Broad Raman scattering structures are found between 3 eV and 10 eV below elastic peaks. They are assigned to be nonbonding type charge transfer excitations or interband transition from O $2p$ valence to Ti $3d$ conduction bands, which includes the crystal field splitting in D_{2h} symmetry with two Ti-O bond lengths.

I. INTRODUCTION

Soft-x-ray fluorescence spectroscopy of solids has been established as a powerful tool to elucidate the partial density of states of the valence band. This process is described as a first order optical process where the correlation between incident and emitted photons is lost. On the other hand, soft-x-ray Raman scattering (SXRS) spectroscopy is a second order optical process, and it gives useful information about the electronic structure of both occupied and unoccupied states. A recent brilliant synchrotron radiation source has enabled one to observe SXRS on semiconductors,[1–5] transition metal compounds,[6–14] and rare earth compounds.[15] The nature of SXRS is basically considered to follow the Kramers-Heisenberg formula. Because the final state of SXRS conserves the electron number N in the system compared with the final state of the photoelectron with the electron number $N-1$, SXRS is not influenced by the core hole effect, so that it is an extremely powerful tool for exploring the electronic structure in the ground state and the electronic excitations. The electronic excitations of SXRS have been interpreted in different ways according to the models of electronic states. In a band model that characterizes an itinerant nature of electrons, electronic excitations are described in terms of an electron-hole pair at a particular symmetric point or a valence exciton by the total momentum conservation rule of a system.[16] In the case of semiconductors, SXRS has been well analyzed by the band calculation. In contrast, in a cluster or atomic model that characterizes the localized nature of electrons, they are described in terms of a $d-d$ or a charge transfer (CT) excitation. SXRS gives direct information on parameter values such as the d-d Coulomb interaction U_{dd}, the hybridization between d and ligand states V_{eff}, or the CT energy Δ, which are often extracted from fitting parameters used in various spectroscopies such as x-ray absorption (XAS), x-ray photoemission (XPS), and so on. SXRS of rare earth compounds have been well analyzed by the localized electron calculation. This is because of the strong electron correlation effect. In the case of transition metal compounds, the electronic structures have been interpreted by the band picture, the localized electron picture, or an intermediate model such as the multisite cluster model,[17] which accounts for translational symmetry in the localized model. Polarization (electric field) dependence of incident and emitted photons has not been included in the previous SXRS measurements, so that the detailed description of elementary excitations in solids is still obscured. For further understanding, it is essential to perform polarization dependence of SXRS (PSXRS) on solids.

Including the polarization vectors of incident and emitted photons, Nakazawa *et al.* have analyzed the fluorescence yield (FY) and SXRS of rare earth metals based on the atomic model.[18] They have shown that the selection rule for PSXRS is followed by the total angular momentum J and its z component J_z. PSXRS gives direct information about the symmetry of each elementary excitation. There exists, however, few previous works on solids where practical measurements and corresponding analysis are performed on PSXRS.[19]

TiO_2 is a representative of a $3d^0$ system, and the character of the electronic states near the energy gap has long been discussed in terms of both delocalized[20–26] and localized[27–32] description. Butorin *et al.* measured Ti $2p$ SXRS of $FeTiO_3$ and found a broad Raman structure around 3–10 eV and a weak Raman peak at 14 eV below recombination peaks.[6] They have applied a localized picture to interpret the SXRS of $FeTiO_3$ by analogy with CeO_2,[14] which is a more localized system with $4f^0$ configuration. On the other hand, Jiménez-Mier *et al.* have applied the energy band model to explain the SXRS of various Ti compounds.[13] They have

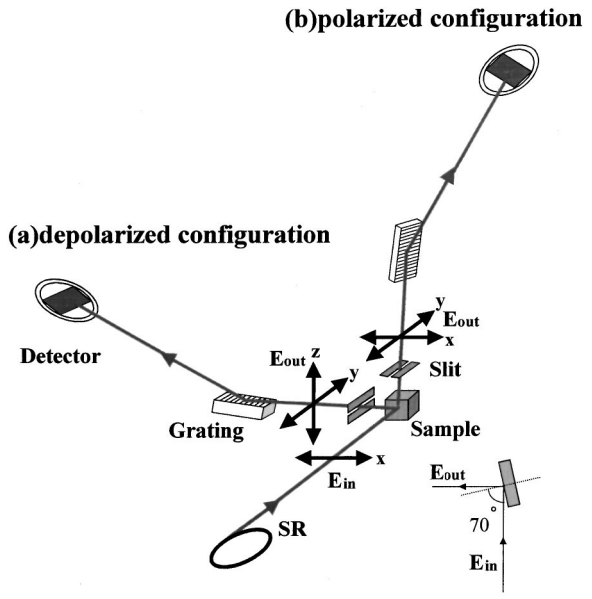

FIG. 1. Experimental setup for PSXRS. (a) Depolarized configuration; the spectrometer is located in the direction of the polarization vector of the incident photon. (b) Polarized configuration; the spectrometer is located normal to the wave vector and the polarization vector of the incident photon.

calculated SXRS by assuming constant transition matrices between the occupied and unoccupied electronic states. They have succeeded in reproducing the general feature of the emission spectra, though complex behavior of Raman scattering and fluorescence with increasing photon energy across the Ti $3d$ edge are not sufficiently explained. In this paper, we present highly energy-resolved experimental results of PSXRS for TiO_2 and discuss whether the band or the local model is better in the interpretation of the data.

II. EXPERIMENTS

Polarized soft-x-ray absorption and emission spectra of a rutile $TiO_2(001)$ single crystal were measured using a soft-x-ray spectrometer[33] installed at the undulator beamline BL-2C (in Photon Factory), at National Laboratory for High Energy Physics.[34] Synchrotron radiation was monochromatized using a varied-line spacing plain grating whose average groove density is 1000 lines/mm. The energy resolution of the incident photon was about 0.4 eV at 450 eV when we measured SXRS and was about 0.1 eV when we measured absorption spectra.

Figure 1 shows the illustration of the experimental system. The incidence angle of the soft x ray was about 70° to avoid the self-absorption effect. The absorption and emission spectra were measured at ''depolarized'' and ''polarized'' configurations. When the SXRS is measured in the depolarized configuration as shown in Fig. 1(a), the polarization vector of the emitted photon rotates by 90° from the polarization vector of the incident photon. On the other hand, when the SXRS is measured in the polarized configuration, as shown in Fig. 1(b), the polarization vector of the emitted photon contains the same polarization vector as that of the incident photon.

Figure 2(a) displays the local bonding nature of titanium

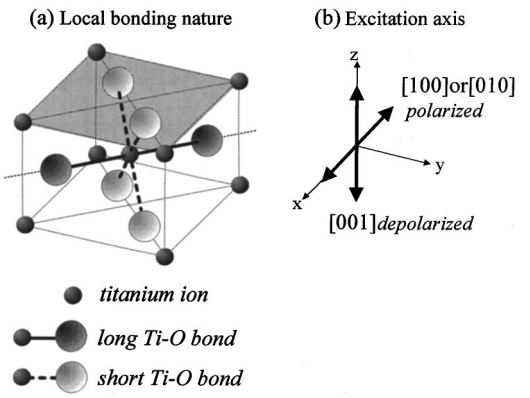

FIG. 2. (a) The local bonding nature of titanium ions with surrounding oxygen ions in rutile TiO_2. (b) The excitation axis for two experimental configurations drawn from the same direction as in (a).

ions with surrounding oxygen ions in rutile TiO_2. The hatched face is in the (001) plane. Rutile has two types of Ti-O bonds: short Ti-O bonds in the (110) or $(1\bar{1}0)$ plane and long Ti-O bonds toward the [110] or $[1\bar{1}0]$ axis. Figure 2(b) shows the polarization vector of the incident photon in the polarized and depolarized configurations. Three axes are chosen so the z axis is parallel to the [001] axis and the xy plane is in the (001) plane. The sample rotates 90° with the experimental chamber so that the excitation axes are different in the polarized and depolarized configurations. As shown in Fig. 2(b), both types of bonds are excited by the incident photons in the polarized configuration, whereas only the short bonds are excited in the depolarized configuration.

The spectrometer is of Rowland mount type with a laminar grating whose radius and groove density are 5 m and 1200 lines/mm. The energy calibration of the incident photon was carried out by the photoemission of gold $4f$ line. For the accurate energy calibration of the spectrometer, we use three elastic scattering lines of TiO_2 to determine the energy scale. The total energy resolution of the system was 0.6 eV at 400 eV with a 20 μm incident slit width of the spectrometer. The base pressure of the experimental chamber was kept below 2×10^{-10} Torr. The measurement time of SXRS was about 300 s for the excitation at the absorption peak and about 1000 s for the excitation below the threshold.

III. RESULTS AND DISCUSSION

The absorption spectra were obtained by the total electron yield method (TEY). Figure 3 shows TEY spectra of TiO_2 excited at Ti $2p$ threshold for the polarized and depolarized configurations. The local symmetry of a titanium ion in the rutile type structure has D_{2h} crystal symmetry, and the structure of TEY is roughly characterized by sharp t_{2g} peaks and double-splitting e_g peaks due to slight distortion from the O_h symmetry. The e_g peak at the lower energy side originates from the long Ti-O bonds due to a hybridization effect weaker than the short Ti-O bonds, so that the intensity ratio of the higher energy to lower energy e_g peaks is slightly increased at the depolarized configuration where the long Ti-O bonds are not excited.

Figure 4 shows the emission spectra excited at selected

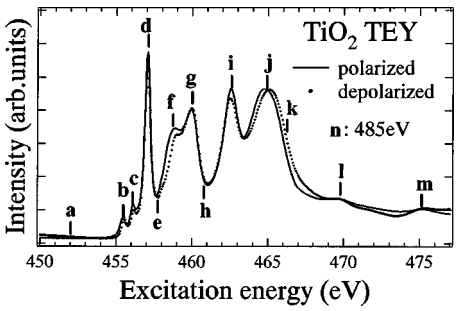

FIG. 3. Total electron yield (TEY) spectrum of TiO_2 at the edge of Ti $2p$. Letters indicate excitation energies for the emission measurement. The continuous and dotted lines show the polarized and depolarized configurations, respectively.

energies as shown by lowercase letters in the TEY spectrum. The spectra are plotted as a function of the emitted photon energy and their intensities are normalized to the incident photon flux. The intensities of polarized and depolarized configurations are normalized so that they coincide in the fluorescence spectra. The highest energy peak in each spectrum is an elastic scattering structure, where the final state is the same as the initial state. From the Kramers-Heisenberg formula, the elastic scattering should be forbidden if the polarization vectors of the incident and emitted photons are perpendicular, as shown later. Then the elastic peaks observed in the spectra in the depolarized configuration may be accompanied by small-energy excitations, such as phonons.

When the Ti $2p$ core electron is excited enough above the

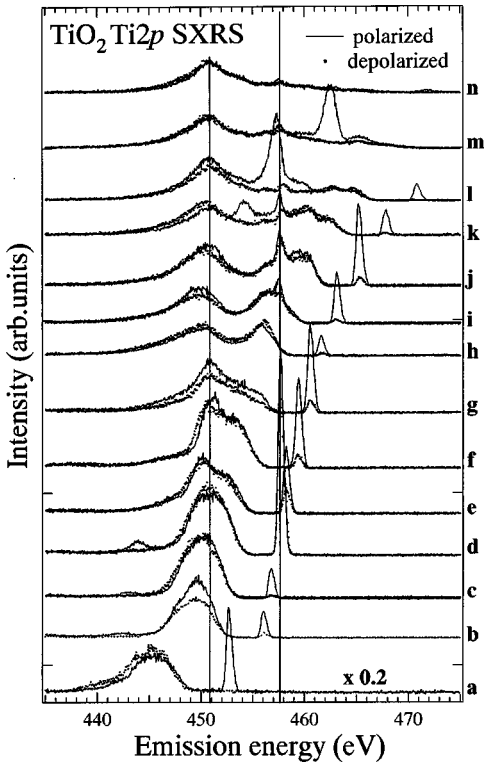

FIG. 4. Polarized soft-x-ray emission spectra of TiO_2. The abscissa is the emitted photon energy. The letters correspond to the excitation energies shown in Fig. 3. The spectrum labeled a is multiplied by 5. Two solid lines at 451 eV and 457.6 eV indicate the peak position of the spectrum labeled n (fluorescence).

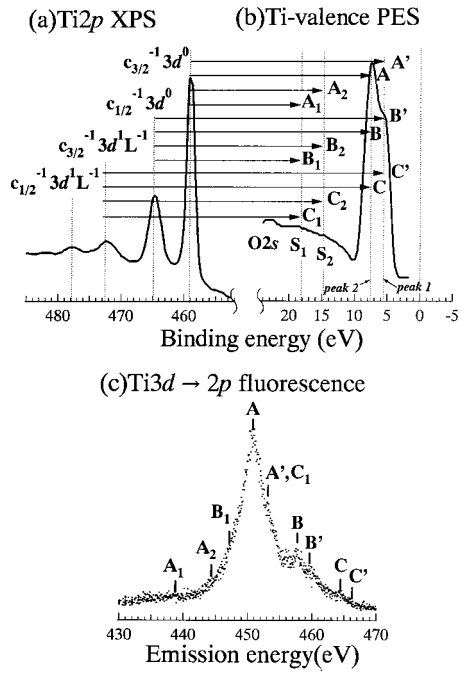

FIG. 5. Assignment of (c) the fluorescence spectrum by comparing the emission energy with the energy difference between the structures of (a) the valence and (b) the Ti $2p$ core photoemission spectra. Corresponding transitions are indicated by the same symbols. Features designated as S_1,S_2 are charge transfer satellites.

continuum state and the excited electron spreads out of the excited core site, one obtains a Ti $3d \rightarrow 2p$ fluorescence spectrum. The multiple-peak structure of the fluorescence is shown in the spectrum labeled **n** (excited enough above the threshold). The Ti $2p$ fluorescence corresponds to the transition from the Ti $2p$ core hole state to the valence hole state, each of which corresponds to the final state of Ti $2p$ and valence-band photoemission, respectively. Therefore it is useful to relate the fluorescence spectra with Ti $2p$ core[29] and valence[30] photoemission spectra as shown in Fig. 5. In Fig. 5(a), for example, $c_{3/2}^{-1}$ denotes a Ti $2p_{3/2}$ core hole and $3d^1L^{-1}$ a Ti $3d$ electron and a hole in the ligand state (O $2p$ molecular orbit). The satellite structures in Ti $2p$ photoemission spectra are located at 472.5 eV and 477.8 eV and have been assigned to the charge transfer type satellites. On the other hand, the valence-band photoemission spectra have been well analyzed by the band structure. However, even in the valence-band photoemission spectra, the charge transfer type satellites S_1 and S_2 are found. The energy of the peaks A and B in the fluorescence spectrum just equals the energy difference between the Ti $2p$ core and valence-band photoemission peaks. Thus, the main structures A, A', B, and B' are elucidated by the valence-band structures. On the other hand, several structures in the fluorescence spectra correspond to the energy positions between the structures involved in the charge transfer satellites. Fluorescence is often described as a first order optical process. Jiménez-Mier *et al.* have explained the fluorescence structure by the calculated projected density of states.[13] They assigned the main peak around 451 eV to the transition from the peak of valence density of states to the Ti $2p_{3/2}$ core state; they also assigned two shoulder structures at the higher energy side to the Coster-Kronig process that transfers the hole from Ti $2p_{1/2}$ to

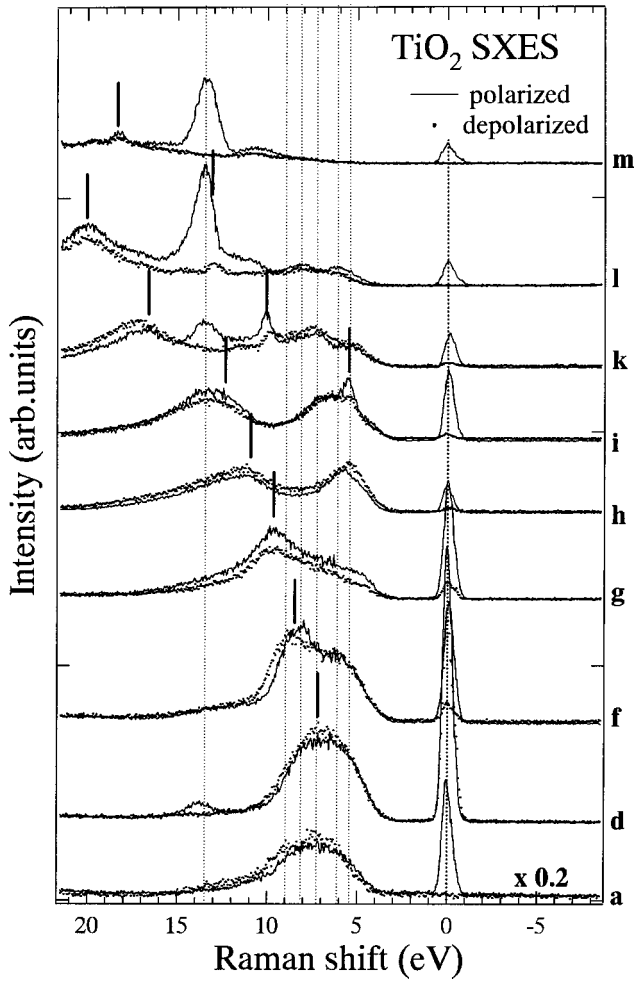

FIG. 6. PSXRS of TiO_2 plotted relative to the elastic peaks located at zero. Five vertical dotted lines between 5 eV and 10 eV indicate Raman scattering to the multiple splitting $3d^1L^{-1}$ nonbonding states, whereas a higher energy shift line around 14 eV indicates Raman scattering to the antibonding state. Solid bars on each spectrum indicate peak positions of the spectrum labeled n (fluorescence).

Ti $2p_{3/2}$ and to a multiple electron excitation, which is consistent with our analysis of peaks *B* and *C*.

In Fig. 4, there are several features that linearly follow with the elastic peaks. Figure 6 shows Raman spectra relative to the energy loss from the elastic peaks. Short bars on each spectrum indicate the energy position of the fluorescence peaks. When the excitation energy is set to the TEY satellite region, dramatic enhancement occurs only at the polarized configuration, that is, the giant enhancement of the 14 eV energy-loss structure as shown by the vertical dotted line in the spectra labeled l and m. Small enhancement is also observed in the spectrum labeled d with a slightly larger Raman shift. This structure has an energy loss that is too large to be associated with valence-band structure but too small to be associated with O $2s$ structure, so that it is difficult to be analyzed using a band calculation. We give, in the following, an interpretation of the observed spectra based on a cluster model.

In the polarized and depolarized configurations, the spectra of SXRS are expressed as

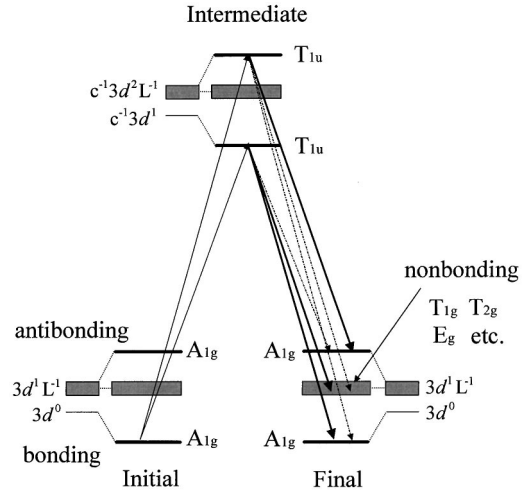

FIG. 7. Schematic energy level diagram for SXRS of TiO_2.

$$F(\Omega,\omega)=\sum_{T_2}\sum_{j}\left|\sum_{i}\frac{\langle j|T_2|i\rangle\langle i|T_1|g\rangle}{E_g+\Omega-E_i-i\Gamma}\right|^2 \times\delta(E_g+\Omega-E_j-\omega), \quad (1)$$

where Ω and ω are, respectively, the incident and emitted photon energies, $|g\rangle$, $|i\rangle$, and $|j\rangle$ are initial, intermediate, and final states of the material system, respectively, E_g, E_i, and E_j are their energies, and Γ represents the spectral broadening due to the core-hole lifetime in the intermediate state. The dipole transition operator T_1 is proportional to *x*, which is taken in the direction of incident photon polarization, and the summation of the dipole transition operator T_2 is taken over *x* and *y* for the polarized configuration, while it is over *y* and *z* for the depolarized configuration (see Fig. 1).

The energy level diagram in the SXRS of TiO_2 is shown schematically in Fig. 7 with a TiO_6 cluster model. TiO_2 is nominally in the $3d^0$ state, but actually the $3d^0$ configuration is strongly mixed with a charge transferred $3d^1L^{-1}$ configuration by the covalency hybridization. The ground state is the bonding state between the $3d^0$ and $3d^1L^{-1}$ configurations, and the antibonding state is located about 14 eV above the ground state with the cluster model parameters used by Okada and Kotani.[35] If we assume, for simplicity, the O_h symmetry for the cluster as done by Okada and Kotani, both bonding and antibonding states are specified by an irreducible representation A_{1g}. In addition to these states, there are nonbonding $3d^1L^{-1}$ states with $A_{2g}, T_{1g}, T_{2g}, E_g, \ldots$ symmetries located near the middle of the bonding and antibonding energy levels. When a Ti $2p$ electron is excited to the $3d$ state by the incident photon, we have $c^{-1}3d^1$ and $c^{-1}3d^2L^{-1}$ configurations that are mixed strongly by the covalency hybridization. The main peak of the Ti $2p$ XAS corresponds to the bonding state between the $c^{-1}3d^1$ and $c^{-1}3d^2L^{-1}$ configurations, while the satellite corresponds to the antibonding state between them. The intensity of the satellite is very weak because of the phase cancellation between the wave functions of the ground and photoexcited states. Also, the x-ray absorption is almost forbidden to the nonbonding $c^{-1}3d^2L^{-1}$ states. In Fig. 7, for simplicity, we disregard the effects of the spin-orbit splitting of the $2p$ states

and the crystal field splitting of the $3d$ states. If we take into account these effects, the main peak (and also the satellite) splits into four peaks.

The resonantly excited intermediate states, which correspond to the main peak and the satellite of the XAS, decay radiatively to each of the final states, i.e., the bonding, nonbonding, and antibonding states. It is easily shown from Eq. (1) and group theoretical consideration that the final states with A_{1g}, T_{1g}, T_{2g}, and E_g irreducible representations are allowed for the polarized configuration, whereas those with only T_{1g} and T_{2g} irreducible representations are allowed for the depolarized configuration. Therefore, the elastic peak (bonding state) and the 14 eV inelastic peak (antibonding state) are allowed for the polarized configuration, but they are forbidden for the depolarized configuration. The nonbonding states are allowed both for the polarized and depolarized configurations. This result is essentially the same, even if we take a cluster with D_{2h} symmetry.

The strong enhancement of the 14 eV peak is qualitatively explained as follows.[15] When the excitation energy is tuned to the TEY satellite structure, the intermediate state is dominated by the antibonding state between $c^{-1}3d^1$ and $c^{-1}3d^2L^{-1}$ configurations. The antibonding intermediate state is likely to decay to another antibonding final state considering the phase matching between wave functions of the ground and photoexcited states, which results in the strong enhancement of the antibonding structure. This is also consistent with the depression of the elastic peak as shown in Fig. 4. The remarkable change of the polarization dependence supports the cluster model with configuration interaction for TiO_2. We have also observed the same enhancement of the antibonding peak in PSXRS of ScF_3.[36]

In Fig. 6, broad structures are observed from 3 to 10 eV below the elastic peaks and are marked with dotted lines. They can be attributed to the Raman scattering structure of $3d^1L^{-1}$ nonbonding states. Nonbonding Raman structures were observed previously[6,10,13] in $3d^0$ compounds, but more structures are resolved in our spectra and exhibit the complex nature of Raman scattering. The spectral shape of them changes considerably as the excitation energy increases. Since the crystal field has the O_h-like symmetry, $3d$ states consist of t_{2g} and double-splitting e_g states, and corresponding Raman peaks may appear in SXRS. The situation is a little more complex if we consider the spatially extended Ti $3d$ states and the delocalized O $2p$ states. As shown in the valence photoemission spectra in Fig. 5, a shoulder appears 2 eV below the main peak. In SXRS we found Raman peaks around 7 eV and 9 eV, which may correspond to the splitting of these bands. This means that nonbonding Raman structures may be elucidated by the band calculation. Very recently, Finkelstein *et al.* have analyzed these nonbonding Raman structures by the full band approach[37] and explained the excitation-energy dependence of them by the restricted joint density of states (RJDOS). It is essentially the same approach as SXRS of semiconductors, where the momentum conservation plays an important role.

The nonbonding Raman structures show clear polarization dependence at the spectra labeled a, d, and f. Raman structures at 7 eV and 9 eV are dominant in the depolarized configuration, whereas the Raman structure at 8 eV is dominant in the polarized configuration (especially in the spectrum labeled f). The polarization dependence of nonbonding structures in solids is an interesting study in SXRS. Figure 8 shows a comparison between SXRS and optical conductivity spectra[38] at two experimental configurations. $\mathbf{E}\|[001]$ and $\mathbf{E}\perp[001]$ in the optical conductivity correspond to depolarized and polarized configuration in SXRS, respectively. An intense peak at 4 eV in the optical conductivity data is interpreted as the exciton peak, and other broad structures below 10 eV split into two regions: those below 6 eV are the transition from O $2p$ nonbonding band to the Ti $3d\,t_{2g}$ states and those above 6 eV are those to the Ti $3d\,e_g$ states. Apart from the intense exciton peak, the energy positions of nonbonding Raman structures correspond well to those of the optical conductivity. Thus it is expected that the difference in Fig. 6 corresponds to the excitation-axis dependence as in the case of TEY. The Raman structures at 7 eV and 9 eV may correspond to the excitation from O $2p$ states to Ti $3d\,e_g$ state originated from short Ti-O bonding. Also, the Raman structure at 8 eV may correspond to the excitation from O $2p$ states to Ti $3d\,e_g$ states originating from long Ti-O bonding. In this way, polarization dependence and excitation energy dependence of highly resolved SXRS will give fruitful information for the valence-band transitions that have been obtained by the optical conductivity in vacuum ultraviolet region.

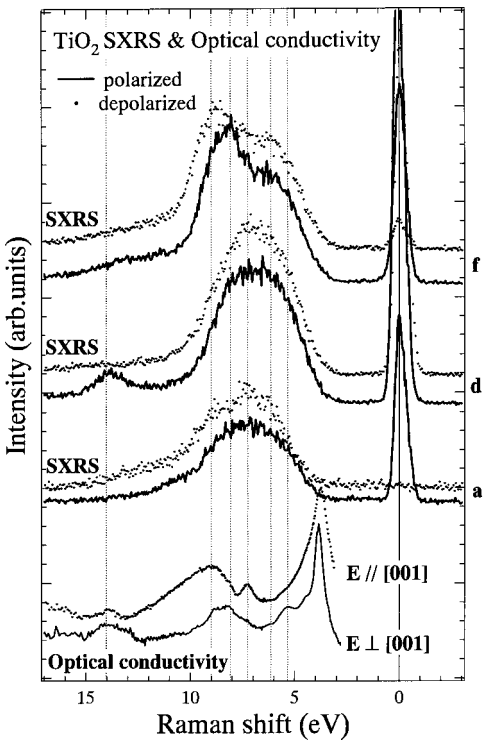

FIG. 8. Energy comparison between nonbonding Raman structures and optical conductivity spectra at two configurations. The spectrum labeled a corresponds to below threshold excitation, and the spectra labeled d and f correspond to the Ti $2p_{3/2}\,t_{2g}$ and e_g excitations, respectively.

IV. CONCLUSIONS

We have measured and analyzed the polarization dependence of the soft-x-ray Raman scattering at the Ti $2p$ absorp-

tion edge of TiO_2. Two types of Raman scattering structures are found, which correspond to the Raman scattering with charge transfer excitations to nonbonding and antibonding states between $3d^0$ and $3d^1L^{-1}$ configurations. The Raman scattering to the antibonding state is clearly enhanced when the incident photon energies are tuned at the TEY satellite. This behavior cannot be explained with band description, whereas it is well reproduced by the configuration interaction cluster calculation of TiO_2. The Raman scattering to the nonbonding states exhibits multiple splitting structures that reflect crystal field splitting of Ti $3d$ electrons and the splitting due to the hybridization effect between the spatially extended Ti $3d$ and nonbonding O $2p$ states. A similar polarization dependence is found in the nonbonding Raman structures and the optical conductivity; thus detailed excitation processes of nonbonding Raman structures are determined. Using highly resolved measurements on SXRS with polarization dependence, it is possible to give evidence to prove both delocalized and localized natures in the ground state of semilocalized electronic systems.

ACKNOWLEDGMENTS

We acknowledge excellent support from the staff of the Photon Factory, KEK. We would like to thank Dr. Sekiya and Professor Kurita for providing unpublished experimental optical conductivity data of TiO_2.

[1] S. Shin, A. Agui, M. Watanabe, M. Fujisawa, Y. Tezuka, and T. Ishii, Phys. Rev. B **53**, 15 660 (1996).
[2] A. Agui, S. Shin, M. Fujisawa, Y. Tezuka, T. Ishii, Y. Muramatsu, O. Mishima, and K. Era, Phys. Rev. B **55**, 2073 (1997).
[3] J.J. Jia, T.A. Callcott, E.L. Shirley, J.A. Carlisle, L.J. Terminello, A. Asfaw, D.L. Ederer, F.J. Himpsel, and R.C.C. Perera, Phys. Rev. Lett. **76**, 4054 (1996).
[4] J.A. Carlisle, E.L. Shirley, E.A. Hudson, L.J. Terminello, T.A. Callcott, J.J. Jia, D.L. Ederer, R.C.C. Perera, and F.J. Himpsel, Phys. Rev. Lett. **74**, 1234 (1995).
[5] Y. Ma, N. Wassdahl, P. Skytt, J. Guo, J. Nordgren, P.D. Johnson, J-E. Rubensson, T. Boske, W. Eberhardt, and S.D. Kevan, Phys. Rev. Lett. **69**, 2598 (1992).
[6] S.M. Butorin, J.-H. Guo, M. Magnuson, and J. Nordgren, Phys. Rev. B **55**, 4242 (1997).
[7] F.M.F. de Groot, P. Kuiper, and G.A. Sawatzky, Phys. Rev. B **57**, 14 584 (1998).
[8] L. Braicovich, C. Dallera, G. Ghiringhelli, N.B. Brookes, J.B. Goedkoop, and M.A. van Veenendaal, Phys. Rev. B **55**, 15 989 (1997).
[9] A. Moewes, D.L. Ederer, M.M. Grush, and T.A. Callcott, Phys. Rev. B **59**, 5452 (1999).
[10] Y. Tezuka, S. Shin, A. Agui, M. Fujisawa, and T. Ishii, J. Phys. Soc. Jpn. **65**, 312 (1996).
[11] S. Shin, M. Fujisawa, H. Ishii, Y. Harada, M. Watanabe, M.M. Grush, T.A. Callcott, R.C.C. Perera, E.Z. Kurmaev, A. Moewes, R. Winarski, S. Stadler, and D.L. Ederer, J. Electron Spectrosc. Relat. Phenom. **92**, 197 (1998).
[12] S.M. Butorin, J.-H. Guo, M. Magnuson, P. Kuiper, and J. Nordgren, Phys. Rev. B **54**, 4405 (1996).
[13] J. Jiménez-Mier, J. van Kd, D.L. Ederer, T.A. Callcott, J.J. Jia, J. Carlisle, L. Terminello, A. Asfaw, and R.C. Perera, Phys. Rev. B **59**, 2649 (1999).
[14] C.-C. Kao, W.A.L. Caliebe, J.B. Hastings, and J.-M. Gillet, Phys. Rev. B **54**, 16 361 (1996).
[15] S.M. Butorin, D.C. Mancini, J.-H. Guo, N. Wassdahl, J. Nordgren, M. Nakazawa, S. Tanaka, T. Uozumi, A. Kotani, Y. Ma, K.E. Miyano, B.A. Karlin, and D.K. Shuh, Phys. Rev. Lett. **77**, 574 (1996).
[16] T. Minami and K. Nasu, Phys. Rev. B **57**, 12 084 (1998).
[17] T. Ide and A. Kotani, J. Phys. Soc. Jpn. **67**, 3621 (1998).
[18] M. Nakazawa, H. Ogasawara, A. Kotani, and P. Lagarde, J. Phys. Soc. Jpn. **67**, 323 (1998).
[19] P. Kuiper, J.-H. Guo, C. Sathe, L.-C. Duda, and J. Nordgren, Phys. Rev. Lett. **80**, 5204 (1998).
[20] Shang-Di Mo and W.Y. Ching, Phys. Rev. B **51**, 13 023 (1995).
[21] B. Poulmellec, P.J. Durham, and G.Y. Guo, J. Phys.: Condens. Matter **3**, 8195 (1991).
[22] N. Daude, C. Gout, and L. Journin, Phys. Rev. B **15**, 3229 (1977).
[23] K. Vos, J. Phys. C **10**, 3917 (1977).
[24] L.B. Lin, S.D. Mo, and D.L. Lin, J. Phys. Chem. Solids **54**, 907 (1993).
[25] A. Hagfeldt, H. Siegbahn, S.-E. Lindquist, and S. Lunell, Int. J. Quantum Chem. **44**, 477 (1992).
[26] M. Cardona and G. Harbeke, Phys. Rev. **137**, A1467 (1965).
[27] S.K. Sen, J. Riga, and J. Verbist, Chem. Phys. Lett. **39**, 560 (1976).
[28] M.A. Khan, A. Kotani, and J.C. Parlebas, J. Phys.: Condens. Matter **3**, 1763 (1991).
[29] T. Jo and A. Tanaka, J. Phys. Soc. Jpn. **64**, 676 (1995).
[30] K.C. Prince, V.R. Dhanak, P. Finetti, J.F. Walsh, R. Davis, C.A. Muryn, H.S. Dhariwal, G. Thornton, and G. van der Laan, Phys. Rev. B **55**, 9520 (1997).
[31] T. Uozumi, K. Okada, and A. Kotani, J. Phys. Soc. Jpn. **62**, 2595 (1993).
[32] Y. Tezuka, S. Shin, T. Ishii, T. Ejima, S. Suzuki, and S. Sato, J. Phys. Soc. Jpn. **63**, 347 (1994).
[33] Y. Harada, H. Ishii, M. Fujisawa, Y. Tezuka, S. Shin, M. Watanabe, Y. Kitajima, and A. Yagishita, J. Synchrotron Radiat. **5**, 1013 (1998).
[34] M. Watanabe, A. Toyoshima, Y. Azuma, T. Hayaishi, Y. Yan, and A. Yagishita, Proc. SPIE **58**, 3150 (1997).
[35] K. Okada and A. Kotani, J. Electron Spectrosc. Relat. Phenom. **62**, 131 (1993).
[36] Y. Harada, H. Ishii, M. Fujisawa, M. Watanabe, A. Yagishita, and S. Shin (unpublished).
[37] L.D. Finkelstein, E.Z. Krumaev, M.A. Korotin, A. Moewes, B. Schneider, S.M. Butorin, J.-H. Guo, J. Nordgren, D. Hartmann, M. Neumann, and D.L. Ederer, Phys. Rev. B **60**, 1 (1999).
[38] T. Sekiya *et al.* (private communication).